

Integrating micro- and nanoelectrodes into atomic force microscopy cantilevers using focused ion beam techniques

A. Lugstein, E. Bertagnolli, C. Kranz, A. Kueng, and B. Mizaikoff

Citation: [Applied Physics Letters](#) **81**, 349 (2002); doi: 10.1063/1.1492304

View online: <http://dx.doi.org/10.1063/1.1492304>

View Table of Contents: <http://scitation.aip.org/content/aip/journal/apl/81/2?ver=pdfcov>

Published by the [AIP Publishing](#)

Articles you may be interested in

[Development of a regeneration-type neural interface: A microtube guide for axon growth of neuronal cells fabricated using focused-ion-beam chemical vapor deposition](#)

J. Vac. Sci. Technol. B **24**, 2538 (2006); 10.1116/1.2359730

[Nanodispenser for attoliter volume deposition using atomic force microscopy probes modified by focused-ion-beam milling](#)

Appl. Phys. Lett. **85**, 6260 (2004); 10.1063/1.1842352

[Three-dimensional and multimaterial microfabrication using focused-ion-beam chemical-vapor deposition and its application to processing nerve electrodes](#)

J. Vac. Sci. Technol. B **22**, 3158 (2004); 10.1116/1.1821581

[A technique to measure Poisson's ratio of ultrathin polymeric films using atomic force microscopy](#)

Rev. Sci. Instrum. **74**, 1043 (2003); 10.1063/1.1531827

[Focused ion beam modification of atomic force microscopy tips for near-field scanning optical microscopy](#)

Appl. Phys. Lett. **79**, 4494 (2001); 10.1063/1.1430028



AIP | Journal of
Applied Physics

Journal of Applied Physics is pleased to
announce **André Anders** as its new Editor-in-Chief

Integrating micro- and nanoelectrodes into atomic force microscopy cantilevers using focused ion beam techniques

A. Lugstein^{a)} and E. Bertagnolli

Solid State Electronics Institute, Vienna University of Technology Floragasse 7, A-1040 Vienna, Austria

C. Kranz, A. Kueng, and B. Mizaikoff

School of Chemistry and Biochemistry, Georgia Institute of Technology, Atlanta, Georgia 30332-0400

(Received 22 January 2002; accepted for publication 21 May 2002)

This paper concerns a scanning probe capable of simultaneously measuring topography and local electrochemistry at a sample surface. Our approach ensures the distance regulation of the electrode by maintaining a fixed working distance between the probe and the sample surface independent from the electrochemical response. This is achieved by integrating micro- and nanoelectrodes into atomic force microscopy tips using focused ion beam techniques. The feasibility and functionality of the fully featured tip is demonstrated by a simultaneous topographical and electrochemical measurement of a porous polymer membrane as model surface. © 2002 American Institute of Physics. [DOI: 10.1063/1.1492304]

Focused ion beam (FIB) methods are among the most promising techniques for three dimensional nanofabrication based on the distinct advantage of a maskless process with unsurpassed flexibility.¹ Bulk micromachining by FIB is commonly used for three dimensional structuring of silicon, e.g., fabrication of ultra sharp atomic force microscopy (AFM) tips and apertures for scanning nearfield optical microscopy tips.² Up to now, this technique has barely found application for the development of electrochemical micro- and nanosystems.³

Scanning electrochemical microscopy (SECM) is a powerful technique for obtaining *in-situ* information on a wide range of processes occurring at interfaces. In the feedback mode, changes of the diffusion-limited Faraday current are recorded at the microelectrode due to hemispherical diffusion of a redox active species present in the electrolyte solution.⁴ Still, a major drawback of this technique is the difficulty in obtaining electrochemical images with a spatial resolution comparable to AFM or scanning tunneling microscopy. In contrast to several approaches described in the literature,^{5–8} this work demonstrates the reproducible integration of micro- and nanoelectrodes into AFM tips utilizing microfabrication techniques. The presented design (Fig. 1) enables simultaneous recording of the topography and electrochemical properties of the sample surface, while the distance between the electrode and the surface remains constant. A detailed description of the measurement setup and quantification of experimental SECM data is given elsewhere.⁹ In order to provide a flexible platform for facile integration into existing AFM instrumentation, standard silicon nitride AFM cantilevers have been modified.

Prior to the deposition of the electrode material the cantilevers were rf sputter coated with a 5 nm adhesion promoting layer of chromium. Subsequently, gold was sputtered

onto the cantilever with a thickness of 60 and 100 nm, respectively. Variation of the metal layer thickness allows adjusting the width of the microfabricated frame-electrode.

Working in electrolytic solutions demands thorough insulation of the electroactive layer, in order to prevent leakage currents interfering with the Faradaic electrochemical response. Therefore, pinhole free insulation of the whole cantilever with the exception of frame-electrode surrounding the AFM tip and a small exposed area of the metal layer at the end of the cantilever mount for the electrical contact is required (see Fig. 1). Insulating $\text{SiO}_2/\text{Si}_3\text{N}_4$ sandwich layers have been deposited by plasma enhanced chemical vapor deposition at 300 °C. Three cycles comprising 5 min Si_3N_4 and subsequent 2 min SiO_2 deposition are completed by 15 min Si_3N_4 layer deposition, corresponding to an overall film thickness of 800 nm. The reliability of the insulating layer was demonstrated by linear-sweep voltammetry.⁹

Integrated micro- and nanoelectrodes require a well-defined working distance of the electroactive area to the sample surface. FIB is used to expose and shape the integrated electrode, and to control the working distance by remodeling of an insulating AFM tip, as illustrated in Fig. 2. FIB modification is a serial process, hence minimizing the processing time for an individual probe is critical. As an improved process with reasonably short etch time, a three-step cut was introduced. All modifications were carried out in a two lens FIB system (Micrion 2500) utilizing a beam of

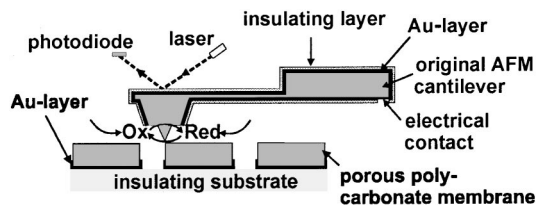


FIG. 1. Schematic illustration of the AFM tip with integrated electrode scanning across a gold coated porous polycarbonate membrane (pore diameter approx. 1 μm) as test sample.

^{a)}Author to whom correspondence should be addressed: electronic mail: alois.lugstein@tuwien.ac.at

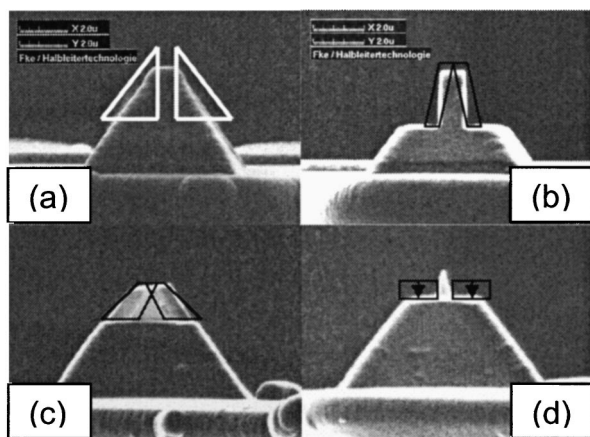


FIG. 2. SEM-FIB images of SECM-AFM tip fabrication. FIB milling steps are schematically indicated.

Ga^+ ions at 50 keV. The first milling steps [depicted in Fig. 2(a)] with a high beam current of 150 pA partly remove the insulating $\text{SiO}_2/\text{Si}_3\text{N}_4$ sandwich layer, the conductive chromium and gold layer and parts of the original Si_3N_4 tip. For the remodeling of a nonconductive AFM tip, additional milling along the indicated lines in Fig. 2(b) was performed at low beam current (45 pA). The FIB image in Fig. 2(c) illustrates the layered structure after a 90° turn of the cantilever and the required cuttings in order to gain an accurately milled tip for high resolution AFM imaging. This process achieves tips with curvatures similar to the initial Si_3N_4 tips and provides comparable topographic imaging quality.⁹

The final fabrication step is a diametrically opposed single pass mill as depicted in Fig. 2(d) at the front side and—after a 90° turn of the cantilever—at the side area of the pyramidal tip, respectively. During single pass mode processing, milling is executed in one frame, with each line in the frame being scanned only once. The scan direction is indicated by the arrows in Fig. 2(d). This final single pass mill flattens the surface and removes redeposited material from the electroactive area of the tip, arising from previous modification steps. Due to the requirements of SECM measurements, the working distance of the electrode can be correlated with the rise of the electroactive surface of the integrated electrode by the length of the remodeled AFM tip. Figs. 3(a) and 3(b) show square frame-shaped electrodes with an edge length of $1.8 \mu\text{m}$ and 650 nm , respectively. The remodeled tip height was adjusted at $1.5 \mu\text{m}$ and 650 nm .

The electrical contact for the integrated electrode is provided by a flattened insulated 0.2-mm -thick copper wire glued with a conducting silver epoxy resin onto the small exposed area of the gold layer at the end of the cantilever

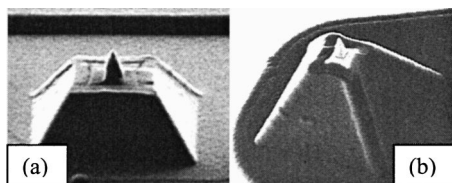


FIG. 3. Integrated square frame shaped electrodes; (a) electrode edge length = $1.8 \mu\text{m}$; tip height = $1.5 \mu\text{m}$; (b) electrode edge length = 650 nm ; tip height = 650 nm .

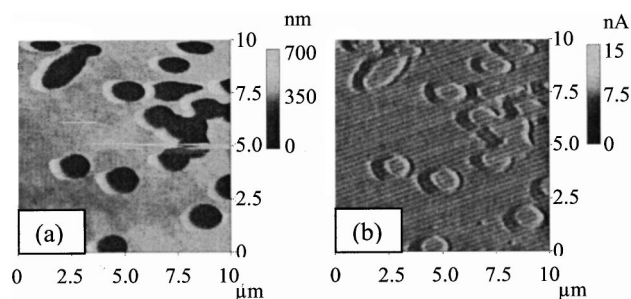


FIG. 4. Simultaneously recorded height and current images of a porous polymer membrane. (a) Top view of the AFM image and (b) top view of the simultaneously recorded current image. Redox mediator: $30 \text{ mM Fe}[\text{CN}]_6^{4-}$ in 0.5 M KCl electrolyte solution, $E_{\text{tip}} = 0.6 \text{ V vs Ag/AgCl}$. Scan parameters: $10 \times 10 \mu\text{m}$, scan rate 2 Hz . Electrode edge length: $1 \mu\text{m}$, remodeled AFM tip: 700 nm .

mount. The contact window was opened by mechanically scratching the isolation layer. After contacting, the cantilever mount was protected by an insulation varnish applied with a fine microbrush.

In order to demonstrate full functionality, the featured integrated SECM-AFM tip was mounted in a standard atomic force microscope (Nanoscope III, Digital Instruments), equipped with a fluid cell in a three-electrode setup with the integrated tip as working electrode, a Pt-electrode as counter electrode and a Ag/AgCl reference electrode. The whole instrument was located in a Faraday cage and the electrochemical experiment was controlled by a bipotentiostat (CH Instruments 832 A). Images were obtained in the contact mode of AFM and feedback mode of SECM.¹⁰

Results of simultaneous topographical and electrochemical measurement are shown in Fig. 4. As a model surface a porous polycarbonate membrane with a thickness of $11 \mu\text{m}$ and an average pore diameter of $1 \mu\text{m}$ was coated with a layer of 50 nm gold at the bottom side. Hence, insulating, conducting, and topographical features are provided at the sample surface. Biasing the integrated tip at a constant potential causes oxidation of the redox mediator in solution (ferrocyanide converted to ferricyanide). As a result, diffusion limited Faradaic current occurs at the tip, which is influenced by the nature of the sample surface. In feedback mode, an insulating surface blocks diffusion to the tip and the tip current decreases, whereas the redox mediator is recycled at a conducting surface, leading to an increased tip current. With the AFM-SECM tip scanning over the insulating polymer, diffusion is blocked, resulting in a decreased current in comparison to the steady-state current in the bulk solution. During imaging of the pores, deposited gold at the edge of the pore causes increase of tip current due to localized regeneration of the redox mediator. Due to the membrane thickness, the remodeled AFM tip does not reach the insulating bottom of the pore, leading to attenuated negative feedback. The topography image shows elevated pore edges in scan direction due to imaging artifacts caused by comparable dimensions of the reshaped tip and the imaged pore features. The corresponding negative feedback observed in the electrochemical image at this location results from the decreased distance of part of the integrated electrode already located over the insulating sample surface, while the reshaped AFM tip is still located in the pore (see Fig. 4). The

comparison of the topographical and the electrochemical image depicted in Fig. 4 shows excellent agreement of the images.

This work was partly supported by the Society for Microelectronics (GME, Austria) and the Austrian Science Foundation (FWF, 14122-CHE). Patents on this technology are pending.^{11,12}

¹J. Melngailis, *J. Vac. Sci. Technol. B* **5**, 469 (1987).

²C. Lehrer, L. Frey, S. Petersen, Th. Sulzbach, O. Ohlsson, and Th. Dziomba, *Microelectron. Eng.* **57**, 721 (2001).

³A. Hoogerwerf and K. D. Wise, *IEEE Trans. Biomed. Eng.* **41**, 1136 (1994).

⁴J. Kwak and A. J. Bard, *J. Anal. Chem.* **61**, 1221 (1989).

⁵D. O. Wipf and A. J. Bard, *Anal. Chem.* **64**, 1362 (1992).

⁶M. Ludwig, C. Kranz, W. Schuhmann, and H. E. Gaub, *Rev. Sci. Instrum.* **66**, 2857 (1995).

⁷P. J. James, L. F. Garfias-Mesias, P. J. Moyer, and W. H. Smyrl, *J. Electrochem. Soc.* **L64**, 145 (1998).

⁸J. V. Macpherson and P. R. Unwin, *Anal. Chem.* **72**, 276 (2000).

⁹C. Kranz, G. Friedbacher, B. Mizaikoff, A. Lugstein, J. Smoliner, and E. Bertagnolli, *Anal. Chem.* **73**, 2491 (2001).

¹⁰A. J. Bard and M. V. Mirkin, *Scanning Electrochemical Microscopy* (Marcel Dekker: New York, 2001), p. 145.

¹¹Patent pending, A 1011/2000 G01N (09 June 2000).

¹²Patent pending, A 1012/2000 G01N (09 June 2000).